HHS Public Access

Author manuscript

Dalton Trans. Author manuscript; available in PMC 2019 July 14.

Published in final edited form as:

Dalton Trans. 2018 July 14; 47(26): 8571–8580. doi:10.1039/c8dt00087e.

Upconversion in Photodynamic Therapy: Plumbing the Depths

Michael R Hamblin*

Wellman Center for Photomedicine, Massachusetts General Hospital, Boston, MA, 02114 USA

Department of Dermatology, Harvard Medical School, Boston, MA 02115, USA

Harvard-MIT Division of Health Sciences and Technology, Cambridge, MA 02139, USA

Abstract

Photodynamic therapy (PDT) involves the combination of non-toxic dyes called photosensitizers (PS) and harmless visible light that interact with ambient oxygen to give reactive oxygen species (ROS) that can damage biomolecules and kill cells. PDT has mostly been developed as a cancer therapy but can also be used as an antimicrobial approach against localized infections. However even the longest wavelength used for exciting PS (in the 700m nm region) has relatively poor tissue penetration, and many PS are much better excited by blue and green light. Therefore upconversion nanoparticles (UCNPs) have been investigated in order to allow deeper-penetrating near-infrared light (980 nm or 810 nm) to be used for PDT. $NaYF_4$ nanoparticles doped with Yb^{3+} and Er^{3+} or with Tm^{3+} and Er^{3+} have been attached to PS either by covalent conjugation, or by absorption to the coating or shell (used to render the UCNPs biocompatible). Forster resonance energy transfer to the PS then allows NIR light energy to be transduced into ROS leading to cell killing and tumor regression. Some studies have experimentally demonstrated the deep tissue advantage of UCNP-PDT. Recent advances have included dye-sensitized UCNPs and UCNPs coupled to PS, and other potentially synergistic drug molecules or techniques. A variety of bioimaging modalities have also been combined with upconversion PDT. Further studies are necessary to optimize the drug-delivery abilities of the UCNPs, improve the quantum yields, allow intravenous injection and tumor targeting, and ensure lack of toxicity at the required doses before potential clinical applications.

Keywords

Photodynamic therapy; upconversion nanoparticles; lanthanide-doped nanocrystals; photosenitizers; near infrared laser; deep tissue light penetration

1. Introduction to photodynamic therapy

Photodynamic therapy (PDT) was discovered in 1900 after a serendipitous observation that single-celled paramecia that were exposed to acridine dyes and light at the same time were killed[1]. Since then a wide range of different photosensitizers (PS) have been developed to mediate PDT of cancer cells, tumors in vivo, and infectious microorganisms[2]. The scientific

* Hamblin@helix.mgh.harvard.edu.

principle involves the absorption of a photon by the ground state PS to boost it to the excited singlet state. This is a very short-lived species (nsec) but can undergo an “intersystem crossing” or spin-flip of the HOMO electron to produce the long-lived triplet state (μsec). The PS triplet life-time is long enough to allow photochemical reactions with ambient oxygen to occur[3]. These reactions can be divided into Type I (electron transfer) yielding superoxide, hydrogen peroxide and hydroxyl radicals, or Type 2 (energy transfer) yielding excited state singlet oxygen. Both these photochemical pathways can occur at the same time, and the balance between them depends on the chemical structure of the PS (particularly the redox potential) and the concentration of ambient oxygen[4]. The reactive oxygen species (ROS) produced then react with biological molecules (nucleic acids, proteins and lipids) eventually causing cell death. Both singlet oxygen ($^1O_2$) and hydroxyl radicals ($HO^\bullet$) are highly reactive oxidants, and therefore tend to react with biomolecules in their immediate vicinity, and therefore their diffusion distance is very short (< 100 nm)[5]. The mechanisms of PDT are schematically illustrated in a Jablonski diagram shown in Figure 1.

Clinical PDT for cancer has mostly been developed whereby the PS is injected intravenously, and after a certain time (the drug-light interval) the tumor is irradiated with red light[6]. It has been well-established that there are three separate mechanisms that operate in this scenario. Firstly, cancer cell death is triggered by the burst of ROS[7]. This cell death has been extensively investigated and is generally characterized as apoptosis or necrosis[8], although paroptosis[9], pro-death autophagy[10], necroptosis[11], and parthanatos[12] have also been described. One of the most important determinants of the type of cell death induced by PDT is the subcellular localization of the PS, whether it be in mitochondria, lysosomes, endoplasmic reticulum, or plasma membrane[13]. Secondly, there is an effect on the microvasculature that supplies the tumor. Both thrombosis and vascular leakage has been described depending on the identity of PS, drug-light interval, fluence rate and overall dose[14]. It should be noted that if the shut-down of the tumor microvasculature is too sudden (i.e. fluence rate is too high) then the abrupt drop in oxygenation within the tumor may be counter-productive, as PDT efficiency depends on having sufficient oxygen available[15]. Thirdly, the acute inflammation and cytokine release induced in the locality of the tumor can activate the innate immune system[16]. Damage-associated molecular patters (DAMPs) resulting from oxidative damage to cellular components can activate neutrophils, macrophages and dendritic cells[17]. Depending on the presence of tumor-associated antigens, and the avoidance of immunosuppressive mechanisms, this activation of the innate immune system may then lead to activation of the adaptive immune system, and production of systemic anti-tumor immunity. This tumor-specific immunity may be sufficiently robust to lead to “spontaneous regression” of distant untreated tumors and induction of long-term memory immunity[18]. These three mechanisms of tumor PDT destruction are schematically illustrated in Figure 2.

One of the important limitations in PDT in vivo (experimental animals or human patients) is the fact that the light needed to excite the PS has a shorter wavelength than is necessary for good tissue penetration. Many innovative approaches have been devised to improve light penetration into tumors, such as the use of interstitial fibers inserted into the tumor[19], optical clearing[20], and short-pulsed lasers that produce transient photobleaching in tissue chromophores[21]. It is a that fact many PS, such as those based on the tetrapyrrole backbone

(porphyrins, chlorins, phthalocyanines) are best excited by blue light (400-430 nm), and green light (490-550 nm). These wavelengths are often significantly better absorbed by the PS, compared to the more often employed red light used in PDT. The inherent limit posed to the efficiency of PDT, by the restricted penetration of visible light into living tissue, has given rise to a number of innovative approaches to circumvent this limitation. Two cutting-edge approaches that will not be covered in this Frontiers article, are (i) the use of X-ray activated nanoparticles that emit visible light (self-lighting PDT)[22], and (ii) two-photon excitation of the PS using very short-pulsed lasers (femtosecond pulse duration) that result in very high peak powers sufficient to give two-photon absorption by the PS[23]. The third approach, which will be covered below is the use of upconversion nanoparticles (UCNPs)[24].

2 Physics and chemistry of upconversion nanoparticles

Lanthanide-doped nanocrystals were introduced as upconversion nanoparticles in the late 1990s[25]. However the basic science behind lanthanide luminescence can be traced back more 150 years ago, when Robert Bunsen carried out a spectroscopic study of “didymium sulfate” crystals[26]. It has been known since the early 1930s that the salts of certain lanthanides were fluorescent[27]. The long lifetime of the excited state due to the spin-forbidden 4f-4f transitions has led to numerous time-resolved fluorescence techniques[28]. One of the first commercial applications of rare earth luminescence was as scintillator screens for use in medical imaging[29]. The phenomenon of upconversion was first discovered by Francois Auzel in 1966[30]. In his PhD thesis research he was working on rare-earth-doped fluorophosphate glasses as laser materials. During this work he observed sequential energy transfers giving rise to the upconversion of infrared to visible light. When he used Yb−Er dopants he obtained green emission and with Yb−Tm he obtained blue emission.

The phenomenon of upconversion is based on an inorganic host crystalline lattice doped with trivalent lanthanide ions such as Yb^{3+}, Er^{3+}, and Tm^{3+}. Lanthanide ions are used because they have multiple 4f excitation levels and completely filled 5s and 5p shells, which shield their 4f electrons, thus producing sharp 4f-4f transition bands with long-lasting excited states (since they are Laporte forbidden). Long lasting excited states provide the longer time necessary for multiple absorptions. By far the most common host material is the transparent salt $NaYF_4$. Other host lattices are $NaGdF_4$ and $NaLuF_4$[31]. The geometric shape of the UCNPs plays a role in determining the efficiency of upconversion, with hexagonal phase nanocrystals displaying higher upconversion emission than cubic-phase crystals[32].

A variety of optical transition processes, including excited-state excitation (ESA) and energy transfer upconversion (ETU) can occur by means of sequential absorption of two or more photons according to the energy states of the dopant ion within the crystalline lattice[33] (see Figure 3). ESA occurs in a single-ion involving sequential absorption of two (or more) photons by an excited ion possessing a real intermediate energy level, and results in promotion of that ion to a higher excited state. In ETU, two photons excite two neighboring ions to a metastable energy level through ground-state absorption. The excited ions then undergo a non-radiative energy transfer, where one reaches the upper excited state the other ion relaxes to the ground state.

UCNPs require the presence of two different dopant ions, one to act as the sensitizer that absorbs the NIR radiation and the other to act as the activator, which emits the visible light. It is generally considered that the concentration of the sensitizer should be higher (~20 mol %) than the concentration of activator (below 2 mol%). The two frequently used rare-earth ion pairs are ytterbium-erbium (Yb^{3+}:Er^{3+}), or ytterbium-thulium (Yb^{3+}:Tm^{3+}). The Yb^{3+} ions function as antennas, to absorb NIR light at around 980 nm and then transfer it to the reciprocal upconverting lanthanide ion. If this ion is Er^{3+}, then green and red emission is observed (Figure 4A), while if the upconverter ion is Tm^{3+}, the emission includes near-ultraviolet, blue and red light (Figure 4B). It is possible to combine both pairings (Yb^{3+}:Er^{3+} and Yb^{3+}:Tm^{3+}) separately doped within the same UCNPs to further widen the range of wavelengths in the luminescence spectrum[34].

To what extent is the increased tissue penetration obtained by long wavelength upconversion important? Indeed, the optical penetration depth of light into skin increases from 1.8 mm at 660 nm, to 2.2 mm at 750 nm and 2.4 mm at 850 nm[35]. Hence, light intensity 10 mm beneath the skin is reduced by a factor of 0.004 at 660 nm, 0.010 at 750 nm and 0.016 at 850 nm. This appears relatively a modest advantage of changing the absorption peak from 660 nm to 910 nm or 810 nm. However, the best wavelength to excite many PS is not in the red wavelengths, but at the Soret band at 400 nm, or at other wavelengths in the blue region (see table 1).

Although the transmission of 980 nm light through tissue is much higher than visible light, there does exist a water absorption peak at 980 nm, which can lead to excessive heating of the tissue at the power levels that are necessary; these can be as high as a few W/cm^2. One solution to overcoming this problem is to include neodymium ions in the UCNPs[36]. Here the Nd^{3+} ions absorb ~800 nm light and transfer the energy to the Yb^{3+} ions that then can transfer the energy to the activator.

The coating that is applied to the outside of the UCNPs is critical to their biological performance. As the size of the crystal decreases, the ratio of the surface area to volume increases dramatically, meaning the dopant ions can be easily quenched due to the effects of surface impurities, ligands, and solvents. Therefore UCNPs require a protective coating such as a typical core-shell structure where the shell is pure $NaYF_4$ and the interior is doped $NaYF_4$. Alternatively methods of applying coatings are techniques known as “ligand exchange” and “bilayer formation”.

When they are synthesized, the UCNPs are covered with organic ligands (usually a long chain fatty acid like oleic acid) that controls the size and shape during preparation. These hydrophobic ligands make the UCNPs water-insoluble and interfere with their biological applications. One simple method to increase solubility in aqueous solvents is ligand exchange, where the hydrophobic native ligand is directly swapped with a more polar hydrophilic ligand, such as polyethyleneglycol (PEG) or polyacrylic acid. However this can be a slow inefficient process and aggregation may occur. A two step procedure involving the removal of the original ligands followed by addition of the hydrophilic ligands, is a better method[37]. The ligand removal step can be a wash with ethanol combined with ultrasonic treatment, or treatment with sodium borohydride or strong acids[37]. Another method of

making a coating involves taking advantage of the existing oleic acid ligands on the surface to build up a pseudo-bilayer[37]. If long amphiphilic alkyl chains are added, these can insert between the existing oleate ligands on the surface of the NP, leaving the hydrophilic head groups to face outwards. Amphiphilic molecules can: (a) undergo strong van-der-Waals interactions; (b) enable the surface charge to be tailored; (c) be sequentially deposited as a layer-by-layer coating. Phospholipids are the best choice as they are very biocompatible and can encourage uptake of the UCNPs by cells. Synthetic amphiphilic polymers can also be used to produce a bilayer[38].

One of the first biological applications of UCNPs was by Chatterjee et al in 2008[39]. These authors prepared 30 nm NPs composed of $NaYF_4$:Yb^{3+}:Er^{3+} and coated them with mesoporous silica and covalently attached folate as a targeting agent. Excitation at 980 nm led to emission peaks at 409, 541 and 656 nm. These UCNPs were tested as fluorescence imaging agents in human HT29 colon, and MCF7 breast carcinoma cells.

3 Upconversion PDT against cancer cells and other targets

As mentioned above the emission spectrum of UCNPs overlaps well with the absorption spectrum of several different classes of PS. The most efficient way of transferring the energy from the UCNPs to the PS is by Forster resonance energy transfer (FRET). FRET operates by energy transfer using non-radiative dipole–dipole coupling[40]. The efficiency of this energy transfer is inversely proportional to the sixth power of the distance between donor and acceptor, making FRET extremely sensitive to small changes in distance. Since the distance between the PS and the UCNP must be very small, and the UCNP must be coated with a biologically compatible coating or shell, it makes sense to use this same coating as the vehicle to load the PS onto the UCNP. This is probably the most often-employed route to prepared PS-loaded UCNP for PDT applications. For instance, a very popular coating is meso-porous silica, and it is well known that meso-SiO_2 has pores with the correct dimensions into which the planar PS molecules can conveniently fit[41]. There is a second possible method to load PS onto the UCNP, namely covalent conjugation. For this route it is necessary to introduce some kind of “chemical handle” to which the actual PS can be covalently attached.

A wide range of different PS has been tested in UCNPs (see table 1 for some examples). The structures of these PS are given in Figure 5. Some workers have used a combination of two different PS each absorbing at different wavelengths in order to maximize the utilization of the upconverted light. One example of this is the combination of zinc-phthalocyanine that absorbs red light (660 nm) and the carbocyanine dye, merocyanine 540 that absorbs 540 nm light [13]. In addition to more traditional PS, there have been reports of titanium dioxide being investigated in UCNPs[42, 43]. Strictly speaking TiO2 operates via a photocatalysis mechanism rather than a PDT mechanism and is more often used for antimicrobial applications[44]. TiO_2 is a large band-gap semi-conductor, which when subjected to light excitation (usually in the UVA spectral region) produces superoxide and hydroxyl radicals via photo-induced electron transfer[45]. Other unconventional PS have also been employed for UCNP-PDT. C60 fullerene is a member of a closed-cage sp2 hybridized carbon nanostructure with a wide absorption spectrum in the visible range and carries out both Type

1 and Type 2 photochemistry[46]. Liu used separately dual-doped (Yb^{3+}:Er^{3+} and Yb^{3+}:Tm^{3+}) UCNPs to take advantage of the broad-spectrum light harvesting ability of fullerenes[34]. Killer Red is a genetically encoded protein developed in Russia in order to photogenerate singlet oxygen[47]. Due to its rather short excitation maximum (around 590 nm) it has been tested in combination with UCNPs by Liang et al[48]. Ultrathin black phosphorus is a relatively new PS that has been reported to have singlet oxygen quantum yields as high as 0.91[49]. It was tested in combination with UCNPs both in vitro and in vivo[50]. A hybrid nanosystem consisting of graphitic carbon nitride combined with graphene quantum dots has been developed to mediate photocatalysis (it acts as a large band-gap semiconductor in a similar manner to TiO_2)[51]. This nanosystem was combined with $NaYF_4$:Yb/Tm UCNPs by Chan et al[52] Many of the studies have used only in vitro cell culture studies, where the main goals are to demonstrate cell uptake of the PS-loaded UCNPs, and cell death upon NIR irradiation. A few studies have attempted to answer the important question, of whether the use of UCNPs really does extend the tissue depth at which PDT can be effective. One study[48] used slabs of pork tissue of varying thickness placed between the laser and the PS loaded cells to demonstrate that the PS-conjugated UCNPs could be effective through deep tissue. When the PS loaded cells were illuminated without any intervening tissue, equal cell killing was obtained with yellow and NIR lasers. However when a 1-cm slab of pork was interspersed on top of the cells, the killing caused by the yellow laser was abolished, while ROS generation shown by microscopy and 60% cell killing still remained with the NIR laser.

Wang et al carried out similar experiments in vivo[53]. They prepared UCNPs (PEG/$NaYF_4$ Yb^{3+}:Er^{3+}) non-covalently loaded with chlorin-e6 (ce6). The UCNPs produced singlet oxygen under excitation by 980 nm laser, although this yield was significantly lower than the singlet oxygen produced by free ce6 at the same concentration excited by red (660 nm) laser. They used mice bearing 4T1 tumors on the back and interspersed an 8-mm slab of pork tissue between the tumor and the laser. Tumors were directly injected with either UCNP-ce6 or free ce6 at the same concentration (1.5 mg/mL), and exposed to 660 nm and 980 nm lasers, respectively, at the same optical power density (0.5 W/cm^2 for 30 min). There was no delay in tumor growth with ce6 excited by 660-nm laser but the group of mice injected with UCNP-Ce6 and excited by 980 nm laser showed a significantly reduced tumor growth rate. Therefore the advantage of UCNP-PDT at a significant tissue depth outweighed the loss of PDT activity (compared to free ce6) caused by construction of the UCNPs-ce6.

One of the limits of UCNPs is the disappointing absorption cross-section of Yb^{3+} at around 975 nm (7×10^{-5} L/g/cm). Compared to typical NIR organic dyes this value is remarkably low, and this is the explanation for the disappointing quantum yields of UCNPs that are sometimes reported. For instance, the comparable absorption cross-section of the IR 806 dye was estimated to be about (390 L/g/cm) or about 5 million times higher[54]. This realization triggered the development of the approach known as dye-sensitized UCNPs[54]. Here a transducing dye is utilized that can transfer excitation energy to the upconverting lanthanide ion (Yb3+) by a similar FRET mechanism to that described above. This energy transfer process produces a big increase in the light-harvesting capability of UCNPs. Wu et al[55] prepared IR806 dye-sensitized β-$NaYF_4$:20%Yb,2% Er@β-$NaYF_4$:10%Yb-UCNPs with a quantum yield (QY) of ~5% at 2 W/cm^2 of 800 nm compared to a QY of only 0.18% at 31

W/cm^2 reported for existing 800 nm excitable UCNPs. These UCNPs were investigated for optogenetic applications by incorporating them into poly(methyl methacrylate) polymer and showing in a model of hippocampal neurons transfected with a red-light responsive channelrhodopsin (ReaChR) that the wavelength of activation could be shifted from 610 nm to 800 nm. This approach also has the additional advantage of converting the 980 nm light into the deeper penetrating 810 nm light as discussed above.

Another issue concerns the quantum yields. The overall quantum yield is a product of the upconversion quantum yield and the FRET transfer quantum yield (FRET efficiency). For a typical PS, it is necessary to consider the triplet quantum yield and the efficiency of energy (or electron) transfer from the dye triplet state to molecular oxygen. The product of these two efficiencies is the quantum yield of ROS generation (QY), which is typically higher than 0.5 for a dye in solution. Even assuming the UCNP and the PS are located at the optimum distance apart, the overall quantum yield is still likely to be rather low.

Dye-sensitized core–shell–shell UCNPs were constructed with IR-808-dye incorporated into the middle shell and $NaGdF_4$:Yb,Er@$NaGdF_4$:Yb@$NaNdF_4$:Yb in the core[56]. Two different PS molecules, merocyanine 540 (MC540) and chlorine(e6) (Ce6) were loaded into the mesoporous silica outer shell to take advantage of both emission wavelengths (550 nm and 650 nm). These UCNPs were tested as PDT agents in HeLa cells in vitro and microscopy (green fluorescence after 808 nm excitation) showed cell uptake, and MTT assay showed greater PDT killing after 808 nm excitation (targeting the IR808 dye) compared to 980 nm excitation (targeting the Yb^{3+} in the UCNPs). In vivo studies used Balb/c mice bearing U14 cervical carcinoma tumors with UCNPs injected intravenously. Trimodal imaging (UC luminescence, MRI and micro-CT based on the metal content) and PDT-mediated tumor inhibition after 808 nm laser irradiation was demonstrated.

4 Multifunctional Upconversion PDT

Some investigators have investigated the possibility of combining UCNP-mediated PDT with an additional moiety in order to improve the overall anti-tumor effect, or to enhance the biocompatibility, provide a tumor targeting ability, or to allow IV delivery.

Active targeting involves the attachment of specific ligands to the nanostructures, which recognize receptors, antigens, or other molecules that are over-expressed on tumors or other tissue types of interest[57]. One of the most important active targeting ligands that has been used for UCNP-mediated PDT, is folate[39, 58–61] (recognizing the folate-receptor alpha that is over-expressed on many cancer types especially ovarian, lung and breast cancer[62]. Hyaluronic acid is another ligand used for active targeting, that recognizes cluster-determinant 44 (CD44), which is overexpressed on many cancer types and also on cancer stem cells[63]. Hyaluronic acid has been used for active targeting of UCNPs by several groups[42, 64–66]. RGD (arginine-glycine-aspartate) is a 3-amino acid motif that is usually incorporated into a cyclic peptide, and which recognizes the alpha V beta 3 integrin (and several other integrins) that are overexpressed on cancer cells and cancer-associated neovascular endothelial cells[67, 68]. RGD has been used by several groups for targeting UCNPs[69–71].

Ai and coworkers prepared PEG-$NaGdF_4$:Yb/Nd@$NaGdF_4$:Yb/Er@$NaGdF_4$ UCNPs covalently conjugated with Rose Bengal and a platinum (IV)chemotherapy drug (c,c,t-$[Pt(NH_3)_2Cl_2{-}(OCOCH_2CH_2NH_2)_2$[72]. This combination led to enhanced cytotoxicity upon irradiation with an 808 nm laser (6 W/cm2 for 5 min) in both wild-type and cisplatin resistant A2780 ovarian cancer cells.

Liu et al studied the combination of UCNP-PDT with a bioreductive drug[73]. The concept of bioreductive drugs takes advantage of tumor hypoxia to convert an inactive prodrug into a potent cytotoxic drug under the action of specific reductase enzymes[74]. Liu's study employed mesoporous silica coated NaYF4:Yb/Er/Gd UCNPs non-covalently co-loaded with the PS (silicon phthalocyanine dihydroxide) and the bioreductive drug (tirapazamine). UCNP-PDT alone gave good control of HeLa tumors in nude mice, while the addition of tirapazamine to the UCNPs significantly improved the overall result.

Chen et al[75] combined mesoSiO_2–coated UCNPs loaded with methylene blue and targeted with folate, and complexed with gold nanorods (AuNRs) in order to take advantage of the surface-enhanced plasmon resonance effect of gold nanostructures in order to improve the efficiency of UCNP-PDT. The addition of the AuNRs produced more singlet oxygen and greater in vitro cell killing than the MB-UCNPs without AuNRs.

Gao et al[76] used a novel approach by modifying their dual PS loaded (ZnPC plus MC540) $NaYF_4$:Yb^{3+},Er^{3+} UCNPs (UCNPs@ SiO_2) with a preparation of mesenchymal stem-cell-membranes. This was done to increase the cancer cell targeting ability, and also to produce a more biocompatible intravenous injectable formulation. These authors had previously investigated this approach for enhancing the delivery of doxorubicin-loaded nanogels to tumors[77]

Wang et al[78] developed a strategy to construct red blood cell (RBC) microcarriers to selectively deliver oxygen to hypoxic tumors to improve PDT with UCNPs. The UCNPs were PEG-NaGdF4:Yb,Er@NaYF4:Yb@NaGdF4:Yb,Nd@NaYF4@NaGdF4:Yb,Tm@NaYF4 that could be excited by both 808 nm and 980 nm lasers. Rose Bengal and avidin were covalently conjugated and a hypoxia sensitive fluorescent probe (HA) was non-covalently attached. RBCs were biotinylated to bind the UCNPs, and folate was inserted into the RBC membrane as a tumor-targeting agent. Irradiation of the final construct with 980 nm led to blue upconverted light which excited the HA probe to emit green fluorescence, which in turn stimulated the RBCs to release oxygen. Next irradiation with 808 nm led to emission of green light to activate the RB for PDT. Intravenous injection into mice followed by dual irradiation of the tumors (808 + 980 nm) led to greater tumor inhibition than with the various controls.

Fan et al[79] constructed a tri-modal UCNP based on a triple approach combining PDT, radiotherapy and chemotherapy that also allowed a bimodal imaging approach (NIR upconversion luminescence and magnetic resonance imaging). The mesoSiO_2-coated $NaYF_4$:Yb/Er/Tm@$NaGdF_4$ UCNPs were co-loaded with the PS, hematoporphyrin and the chemotherapy drug doxorubicin. Both of these compounds are able to act as radio-

sensitizers to increase the effect of X-ray therapy. Intravenous injection of these UCNPs into BALB/c mice bearing 4T1 tumors followed by application of X-rays (8 Gy over 5 min) and 980 nm laser (2.5 W/cm^2 for 30 min). The triple combination produced better tumor response than the single and dual controls. The same group constructed another multifunctional UCNP-based system[80]. The same mesoSiO$_2$-coated NaYF$_4$:Yb/Er/Tm@NaGdF$_4$ UCNPs described above were co-loaded with two different PS, PPIX and SPCD, and then TAT peptide was attached to the outside of the UCNP to stimulate cell uptake and provide a nuclear-targeting capability. Dual irradiation of tumors with 980 nm laser and X-rays carried out $^1O_2$ generation for PDT, as well as HO● generation produced by PPIX-radiosensitized radiolysis of water by X-rays[81].

Xu et al[82] investigated the combination of UCNP-PDT with immune modulation to enhance the anticancer immune response. They used two separate strategies combined with PEG-NaYF$_4$:Yb^{3+},Er^{3+} UCNPs non-covalently loaded with ce6. Firstly the small molecule Toll-like receptor 7 agonist imiquimod was co-loaded into the UCNPs. These combination UCNPs produced greater activation of bone-marrow-derived dendritic cells (as judged by IL12 and TNFalpha secretion) than free imiquimod alone. Secondly they used a checkpoint inhibitor (anti-CTLA4 antibody) that inhibits immunosuppressive regulatory T cells[83]. CT26 colorectal tumors were implanted in BALB/c mice and UCNP-Ce6-imiquimod was intratumorally injected followed 2 hours later by irradiation with a 980 nm NIR laser (0.5 W/cm^2 for 30 min). Anti-CTLA4 antibody was intravenously injected on days 9 and 13. The triple combination (UCNP-PDT, imiquimod, anti-CTLA4) produced a greater anti-tumor response than any of the control groups (single and dual), and moreover, distant untreated tumors underwent spontaneous regression and cured mice rejected a second challenge with tumor cells.

5 Future outlook

The nanomedicine revolution has resulted in a large variety of novel approaches to enhance PDT. Many of these approaches have been concerned with attempts to improve the delivery of PS, which in addition to poor aqueous solubility, have a pronounced tendency to aggregate in biological media[84]. Liposomes, micelles, mesoporous silica NPs, self-assembled polymeric NPs, have all shown advantages in PDT[85]. However as we have seen above, one application of nanomedicine has the potential to overcome two separate drawbacks of PDT at the same time. It is theoretically possible that a well-designed UCNP could solubilize and disaggregate the PS, while at the same time transducing deep-penetrating NIR light into shorter wavelength visible light to efficiently excite the PS. However, considerable progress will be needed before this dream becomes a reality. Firstly, the type of nanoparticles employed for upconversion are broadly different from those which have been shown to improve the physicochemical properties of PS. Covalent conjugation tends to lower the quantum yields of most PS, due to the restriction of the molecular movement and higher self-quenching. The non-covalent adsorption of PS into UCNP coatings such as PEG and mesoporous silica may not be optimal for PS disaggregation and the quantum yield may be lowered. The second problem that will need to be addressed is the mode of delivery in vivo. It is quite well-established that direct intratumoral injection (as is frequently employed for UCNPs) is not optimal for anti-cancer PDT. The PS does not easily

gain access to the microvasculature when directly injected into the tumor, so the vascular shut-down ingredient of the anti-tumor effect of PDT tends to be lost. Thirdly we have potential toxicity problems of the constituent lanthanide ions in the nanocrystals. A review on the biosafety of upconversion nanomaterials was recently published[86]. While it does not appear that the toxicity of these UCNPs is particularly worrying as far as nanotoxicology goes, it should be remembered that the dosage necessary for carrying out PDT may be substantially higher than the dose employed for imaging studies. For instance one study claimed that 15 mg/kg of PAA-coated $NaYF_4$:Yb,Er UCNPs injected intravenously was a "high dose"[87]. This dose exhibited no toxicity However the IV injected dose of free ce6 in mouse PDT experiments is usually fixed at 10 mg/kg[6]. A few reports have provided the wt/wt ratio of PS to UCNP as 10%[88] or 8%[53]. While free ce6 is not particularly efficient after IV injection, it does give a comparable indication of what dose of UCNPs may be required, considering the reduction in QY typical of upconversion (dose could be >100 mg/kg). This level of dose may pose risks of toxicity occurring. Nevertheless, the conclusion is, that since the basic principle of the increase in effective depth of tissue destruction obtainable by UCNP-PDT, has been demonstrated in studies that have shown that the NIR laser can be effective through interspersed slabs of pork tissue, further research is therefore worth pursuing in this intriguing direction.

Acknowledgments

Michael R Hamblin was supported by US NIH grants R01AI050875 and R21AI121700.

References

1. Moan J, Peng Q. Anticancer Res. 2003; 23:3591–3600. [PubMed: 14666654]
2. Abrahamse H, Hamblin MR. Biochem J. 2016; 473:347–364. [PubMed: 26862179]
3. Ochsner M. J Photochem Photobiol B. 1997; 39:1–18. [PubMed: 9210318]
4. Garcia-Diaz M, Huang YY, Hamblin MR. Methods. 2016; 109:158–166. [PubMed: 27374076]
5. Kochevar IE. Sci STKE. 2004; 2004:pe7. [PubMed: 14983102]
6. Boyle RW, Dolphin D. Photochem Photobiol. 1996; 64:469–485. [PubMed: 8806226]
7. Mroz P, Yaroslavsky A, Kharkwal GB, Hamblin MR. Cancers (Basel). 2011; 3:2516–2539. [PubMed: 23914299]
8. Plaetzer K, Kiesslich T, Oberdanner CB, Krammer B. Curr Pharm Des. 2005; 11:1151–1165. [PubMed: 15853663]
9. Kessel D, Oleinick NL. Photochem Photobiol. 2017; doi: 10.1111/php.12857
10. Kessel D. Autophagy. 2015; 11:1941–1943. [PubMed: 26313747]
11. Miki Y, Akimoto J, Moritake K, Hironaka C, Fujiwara Y. Lasers Med Sci. 2015; 30:1739–1745. [PubMed: 26109138]
12. Soriano J, Mora-Espi I, Alea-Reyes ME, Perez-Garcia L, Barrios L, Ibanez E, Nogues C. Sci Rep. 2017; 7:41340. [PubMed: 28112275]
13. Buytaert E, Dewaele M, Agostinis P. Biochim Biophys Acta. 2007; 1776:86–107. [PubMed: 17693025]
14. Busch TM. Lasers Surg Med. 2006; 38:494–499. [PubMed: 16788920]
15. Henderson BW, Busch TM, Snyder JW. Lasers Surg Med. 2006; 38:489–493. [PubMed: 16615136]
16. Castano AP, Mroz P, Hamblin MR. Nat Rev Cancer. 2006; 6:535–545. [PubMed: 16794636]
17. Garg AD, Krysko DV, Vandenabeele P, Agostinis P. Photochem Photobiol Sci. 2011; 10:670–680. [PubMed: 21258717]

18. Mroz P, Szokalska A, Wu MX, Hamblin MR. PLoS One. 2010; 5:e15194. [PubMed: 21179470]
19. Shafirstein G, Bellnier D, Oakley E, Hamilton S, Potasek M, Beeson K, Parilov E. Cancers (Basel). 2017; 9
20. Pires L, Demidov V, Vitkin IA, Bagnato V, Kurachi C, Wilson BC. J Biomed Opt. 2016; 21:081210. [PubMed: 27300502]
21. Pogue BW, Momma T, Wu HC, Hasan T. Br J Cancer. 1999; 80:344–351. [PubMed: 10408836]
22. Rimoldi T, Orsi D, Lagonegro P, Ghezzi B, Galli C, Rossi F, Salviati G, Cristofolini L. J Mater Sci Mater Med. 2016; 27:159. [PubMed: 27637929]
23. Starkey JR, Rebane AK, Drobizhev MA, Meng F, Gong A, Elliott A, McInnerney K, Spangler CW. Clin Cancer Res. 2008; 14:6564–6573. [PubMed: 18927297]
24. Idris NM, Jayakumar MK, Bansal A, Zhang Y. Chem Soc Rev. 2015; 44:1449–1478. [PubMed: 24969662]
25. Boyer JC, Vetrone F, Cuccia LA, Capobianco JA. J Am Chem Soc. 2006; 128:7444–7445. [PubMed: 16756290]
26. Bunsen R. The Philosophical Magazine: A Journal of Theoretical Experimental and Applied Physics. 1864; 28:246–247.
27. Bunzli JC. Chem Rev. 2010; 110:2729–2755. [PubMed: 20151630]
28. Yuan J, Wang G. J Fluoresc. 2005; 15:559–568. [PubMed: 16167214]
29. Cavouras D, Kandarakis I, Panayiotakis GS, Evangelou EK, Nomicos CD. Med Phys. 1996; 23:1965–1975. [PubMed: 8994161]
30. Auzel F. Chem Rev. 2004; 104:139–173. [PubMed: 14719973]
31. Yin D, Song K, Ou Y, Wang C, Liu B, Wu M. J Nanosci Nanotechnol. 2013; 13:4162–4167. [PubMed: 23862466]
32. Krämer KW, Biner D, Frei G, Güdel KU, Hehlen MP, Lüthi SR. Chemistry of Materials. 2004; 16:1244–1251.
33. Sivakumar S, van Veggel FC, May PS. J Am Chem Soc. 2007; 129:620–625. [PubMed: 17227025]
34. Liu X, Zheng M, Kong X, Zhang Y, Zeng Q, Sun Z, Buma WJ, Zhang H. Chem Commun (Camb). 2013; 49:3224–3226. [PubMed: 23482948]
35. Bashkatov AN, Genina EA, Kochubey VI, Tuchin VV. Journal of Physics D: Applied Physics. 2005; 38:2543.
36. Shen J, Chen G, Vu AM, Fan W, Bilsel OS, Chang CC, Han G. Advanced Optical Materials. 2013; 1:644–650.
37. Muhr V, Wilhelm S, Hirsch T, Wolfbeis OS. Acc Chem Res. 2014; 47:3481–3493. [PubMed: 25347798]
38. Yang S, Li N, Liu Z, Sha W, Chen D, Xu Q, Lu J. Nanoscale. 2014; 6:14903–14910. [PubMed: 25362857]
39. Chatterjee DK, Yong Z. Nanomedicine (Lond). 2008; 3:73–82. [PubMed: 18393642]
40. Ad N, Oron U. Int J Cardiol. 2001; 80:109–116. [PubMed: 11578700]
41. Wang Y, Zhao Q, Han N, Bai L, Li J, Liu J, Che E, Hu L, Zhang Q, Jiang T, Wang S. Nanomedicine. 2015; 11:313–327. [PubMed: 25461284]
42. Hou Z, Deng K, Li C, Deng X, Lian H, Cheng Z, Jin D, Lin J. Biomaterials. 2016; 101:32–46. [PubMed: 27267626]
43. Lucky SS, Muhammad Idris N, Li Z, Huang K, Soo KC, Zhang Y. ACS Nano. 2015; 9:191–205. [PubMed: 25564723]
44. Wang W, Huang G, Yu JC, Wong PK. J Environ Sci (China). 2015; 34:232–247. [PubMed: 26257366]
45. Foster HA, Ditta IB, Varghese S, Steele A. Appl Microbiol Biotechnol. 2011; 90:1847–1868. [PubMed: 21523480]
46. Huang YY, Sharma SK, Yin R, Agrawal T, Chiang LY, Hamblin MR. J Biomed Nanotechnol. 2014; 10:1918–1936. [PubMed: 25544837]

47. Shirmanova M, Yuzhakova D, Snopova L, Perelman G, Serebrovskaya E, Lukyanov K, Turchin I, Subochev P, Lukyanov S, Kamensky V, Zagaynova E. PLoS One. 2015; 10:e0144617. [PubMed: 26657001]
48. Liang L, Lu Y, Zhang R, Care A, Ortega TA, Deyev SM, Qian Y, Zvyagin AV. Acta Biomater. 2017; 51:461–470. [PubMed: 28063989]
49. Lv R, Yang D, Yang P, Xu J, He F, Gai S, Li C, Dai Y, Yang G, Lin J. Chem Mater. 2016; 2016:4724–4734.
50. Wang H, Yang X, Shao W, Chen S, Xie J, Zhang X, Wang J, Xie Y. J Am Chem Soc. 2015; 137:11376–11382. [PubMed: 26284535]
51. Rajender G, Choudhury B, Giri PK. Nanotechnology. 2017; 28:395703. [PubMed: 28726671]
52. Chan MH, Chen CW, Lee IJ, Chan YC, Tu D, Hsiao M, Chen CH, Chen X, Liu RS. Inorg Chem. 2016; 55:10267–10277. [PubMed: 27667449]
53. Wang C, Tao H, Cheng L, Liu Z. Biomaterials. 2011; 32:6145–6154. [PubMed: 21616529]
54. Wang X, Valiev RR, Ohulchanskyy TY, Agren H, Yang C, Chen G. Chem Soc Rev. 2017; doi: 10.1039/c7cs00053g
55. Wu X, Zhang Y, Takle K, Bilsel O, Li Z, Lee H, Zhang Z, Li D, Fan W, Duan C, M Chan E, Lois C, Xiang Y, Han G. ACS Nano. 2016; 10:1060–1066. [PubMed: 26736013]
56. Xu J, Yang P, Sun M, Bi H, Liu B, Yang D, Gai S, He F, Lin J. ACS Nano. 2017; 11:4133–4144. [PubMed: 28320205]
57. Chitgupi U, Qin Y, Lovell JF. Nanotheranostics. 2017; 1:38–58. [PubMed: 29071178]
58. Cui S, Yin D, Chen Y, Di Y, Chen H, Ma Y, Achilefu S, Gu Y. ACS Nano. 2013; 7:676–688. [PubMed: 23252747]
59. Wang C, Cheng L, Liu Z. Biomaterials. 2011; 32:1110–1120. [PubMed: 20965564]
60. Wang H, Liu Z, Wang S, Dong C, Gong X, Zhao P, Chang J. ACS Appl Mater Interfaces. 2014; 6:3219–3225. [PubMed: 24511877]
61. Yang C, Liu Q, He D, Na N, Zhao Y, Ouyang J. Analyst. 2014; 139:6414–6420. [PubMed: 25327945]
62. Cheung A, Bax HJ, Josephs DH, Ilieva KM, Pellizzari G, Opzoomer J, Bloomfield J, Fittall M, Grigoriadis A, Figini M, Canevari S, Spicer JF, Tutt AN, Karagiannis SN. Oncotarget. 2016; 7:52553–52574. [PubMed: 27248175]
63. Wickens JM, Alsaab HO, Kesharwani P, Bhise K, Amin M, Tekade RK, Gupta U, Iyer AK. Drug Discov Today. 2017; 22:665–680. [PubMed: 28017836]
64. Wang X, Yang CX, Chen JT, Yan XP. Anal Chem. 2014; 86:3263–3267. [PubMed: 24621215]
65. Zhou J, Luo P, Sun C, Meng L, Ye W, Chen S, Du B. Nanoscale. 2017; 9:4244–4254. [PubMed: 28291267]
66. Zhou L, Chen E, Jin W, Wang Y, Zhou J, Wei S. Dalton Trans. 2016; 45:15170–15179. [PubMed: 27711660]
67. Sun CC, Qu XJ, Gao ZH. Am J Ther. 2016; 23:e198–207. [PubMed: 24621642]
68. Rubtsov MA, Syrkina MS, Aliev G. Curr Pharm Des. 2016; 22:932–952. [PubMed: 26648463]
69. Gao W, Wang Z, Lv L, Yin D, Chen D, Han Z, Ma Y, Zhang M, Yang M, Gu Y. Theranostics. 2016; 6:1131–1144. [PubMed: 27279907]
70. Zhou A, Wei Y, Chen Q, Xing D. J Biomed Nanotechnol. 2015; 11:2003–2010. [PubMed: 26554158]
71. Zhou A, Wei Y, Wu B, Chen Q, Xing D. Mol Pharm. 2012; 9:1580–1589. [PubMed: 22533630]
72. Ai F, Sun T, Xu Z, Wang Z, Kong W, To MW, Wang F, Zhu G. Dalton Trans. 2016; 45:13052–13060. [PubMed: 27430044]
73. Liu Y, Liu Y, Bu W, Cheng C, Zuo C, Xiao Q, Sun Y, Ni D, Zhang C, Liu J, Shi J. Angew Chem Int Ed Engl. 2015; 54:8105–8109. [PubMed: 26012928]
74. Phillips RM. Expert Opin Investig Drugs. 1998; 7:905–928.
75. Chen CW, Chan YC, Hsiao M, Liu RS. ACS Appl Mater Interfaces. 2016; 8:32108–32119. [PubMed: 27933825]

76. Gao C, Lin Z, Wu Z, Lin X, He Q. ACS Appl Mater Interfaces. 2016; 8:34252–34260. [PubMed: 27936561]
77. Gao C, Lin Z, Jurado-Sanchez B, Lin X, Wu Z, He Q. Small. 2016; 12:4056–4062. [PubMed: 27337109]
78. Wang P, Li X, Yao C, Wang W, Zhao M, El-Toni AM, Zhang F. Biomaterials. 2017; 125:90–100. [PubMed: 28235648]
79. Fan W, Shen B, Bu W, Chen F, He Q, Zhao K, Zhang S, Zhou L, Peng W, Xiao Q, Ni D, Liu J, Shi J. Biomaterials. 2014; 35:8992–9002. [PubMed: 25103233]
80. Fan W, Shen B, Bu W, Zheng X, He Q, Cui Z, Ni D, Zhao K, Zhang S, Shi J. Biomaterials. 2015; 69:89–98. [PubMed: 26283156]
81. Takahashi J, Misawa M. Radiation Physics and Chemistry. 2009; 78:889–898.
82. Xu J, Xu L, Wang C, Yang R, Zhuang Q, Han X, Dong Z, Zhu W, Peng R, Liu Z. ACS Nano. 2017; 11:4463–4474. [PubMed: 28362496]
83. Wing K, Onishi Y, Prieto-Martin P, Yamaguchi T, Miyara M, Fehervari Z, Nomura T, Sakaguchi S. Science. 2008; 322:271–275. [PubMed: 18845758]
84. Master A, Livingston M, Sen Gupta A. J Control Release. 2013; 168:88–102. [PubMed: 23474028]
85. Avci P, Erdem SS, Hamblin MR. J Biomed Nanotechnol. 2014; 10:1937–1952. [PubMed: 25580097]
86. Sun Y, Feng W, Yang P, Huang C, Li F. Chem Soc Rev. 2015; 44:1509–1525. [PubMed: 25113504]
87. Xiong L, Yang T, Yang Y, Xu C, Li F. Biomaterials. 2010; 31:7078–7085. [PubMed: 20619791]
88. Shan JN, Budijono SJ, Hu GH, Yao N, Kang YB, Ju YG, Prud'homme RK. Adv Funct Mater. 2011; 21:2488–2495.
89. Guo H, Qian H, Idris NM, Zhang Y. Nanomedicine. 2010; 6:486–495. [PubMed: 20044035]
90. Idris NM, Gnanasammandhan MK, Zhang J, Ho PC, Mahendran R, Zhang Y. Nat Med. 2012; 18:1580–1585. [PubMed: 22983397]
91. Yuan Q, Wu Y, Wang J, Lu D, Zhao Z, Liu T, Zhang X, Tan W. Angew Chem Int Ed Engl. 2013; 52:13965–13969. [PubMed: 24281972]
92. Khaydukov EV, Mironova KE, Semchishen VA, Generalova AN, Nechaev AV, Khochenkov DA, Stepanova EV, Lebedev OI, Zvyagin AV, Deyev SM, Panchenko VY. Sci Rep. 2016; 6:35103. [PubMed: 27731350]
93. Li S, Cui S, Yin D, Zhu Q, Ma Y, Qian Z, Gu Y. Nanoscale. 2017; 9:3912–3924. [PubMed: 28261736]
94. Wang D, Xue B, Kong X, Tu L, Liu X, Zhang Y, Chang Y, Luo Y, Zhao H, Zhang H. Nanoscale. 2015; 7:190–197. [PubMed: 25406514]
95. Choi SY, Baek SH, Chang SJ, Song Y, Rafique R, Lee KT, Park TJ. Biosens Bioelectron. 2017; 93:267–273. [PubMed: 27590213]

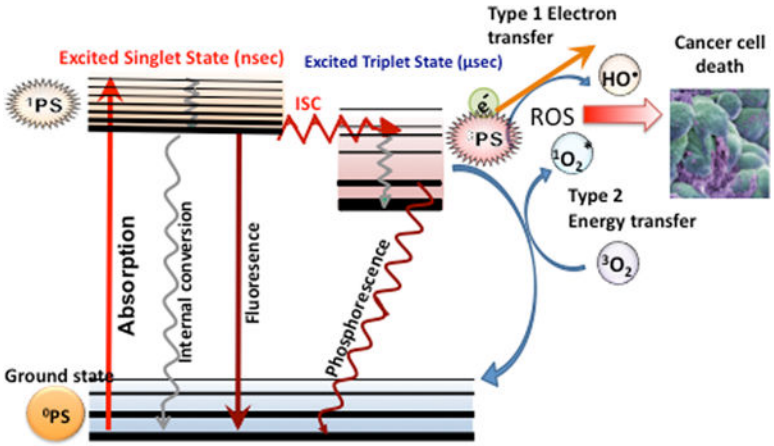

Figure 1. Jablonski diagram illustrating the principles of PDT

A ground-state photosensitizer (^{0}PS) absorbs a photon, transitions to the short-lived (nsec) excited singlet state (^{1}PS) that can lose energy by fluorescence, internal conversion to heat, or else can undergo intersystem crossing to the long-lived (µsec) excited triplet state (^{3}PS). The^{3}PS can relax to ground state by emitting phosphorescence, but can also undergo energy transfer with ground state triplet oxygen ($^3O_2$) to form reactive singlet oxygen ($^1O_2$, Type 2) or else can undergo an electron transfer reaction to form hydroxyl radicals (HO•, Type 1). Both these ROS ($^1O_2$ and HO•) can efficiently kill cancer cells (see Figure 2).

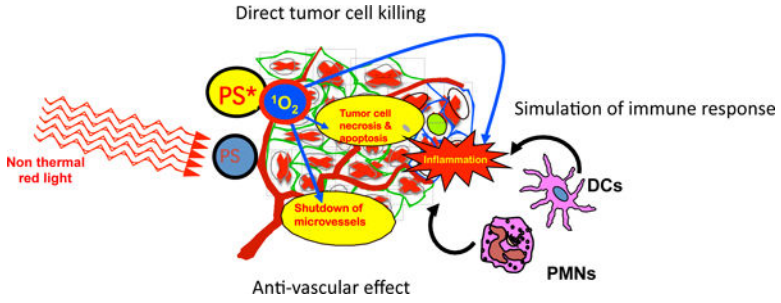

Figure 2. Schematic illustration of the three mechanisms responsible for the PDT-mediated destruction of a tumor in vivo

Photosensitizer (PS) absorbs light and is excited to the long-lived triplet state PS* which produces excited state singlet oxygen $^1O_2$. $^1O_2$ can (1) directly kill tumor cells by necrosis and induction of apoptosis, (2) can cause destruction of tumor vasculature by shutting down microvessels, and (3) can produce an acute inflammatory response that attracts leukocytes such as dendritic cells (DC) and neutrophils (PMN) that stimulates immune response.

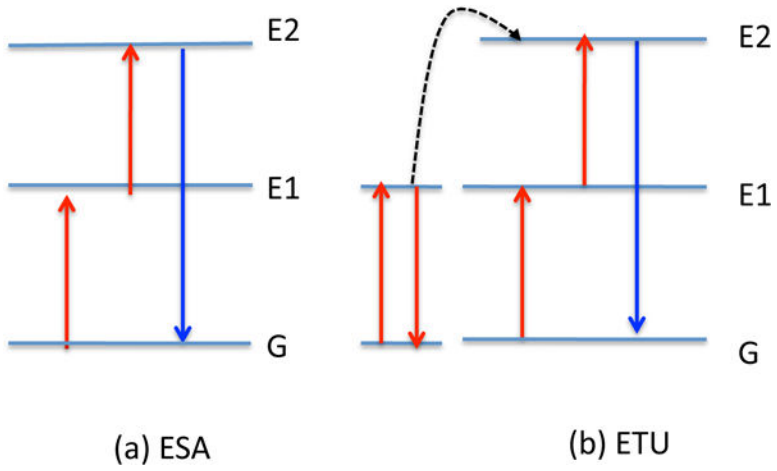

Figure 3. Two common energy transfer processes occurring in upconversion
(A) ESA, excited-state excitation; (B) ETU, energy transfer upconversion.

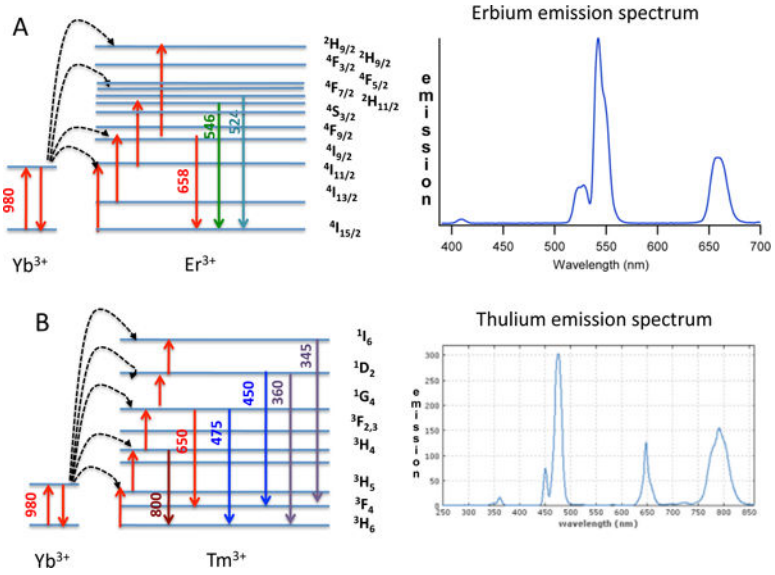

Figure 4. Emission spectra and energy levels of the two common types of UCNPs

(A) The Yb3+ and Er3+ pairing emitting green, red and NIR light

(B) The Yb3+ and Tm3+ pairing emitting UVA, blue, red and NIR light

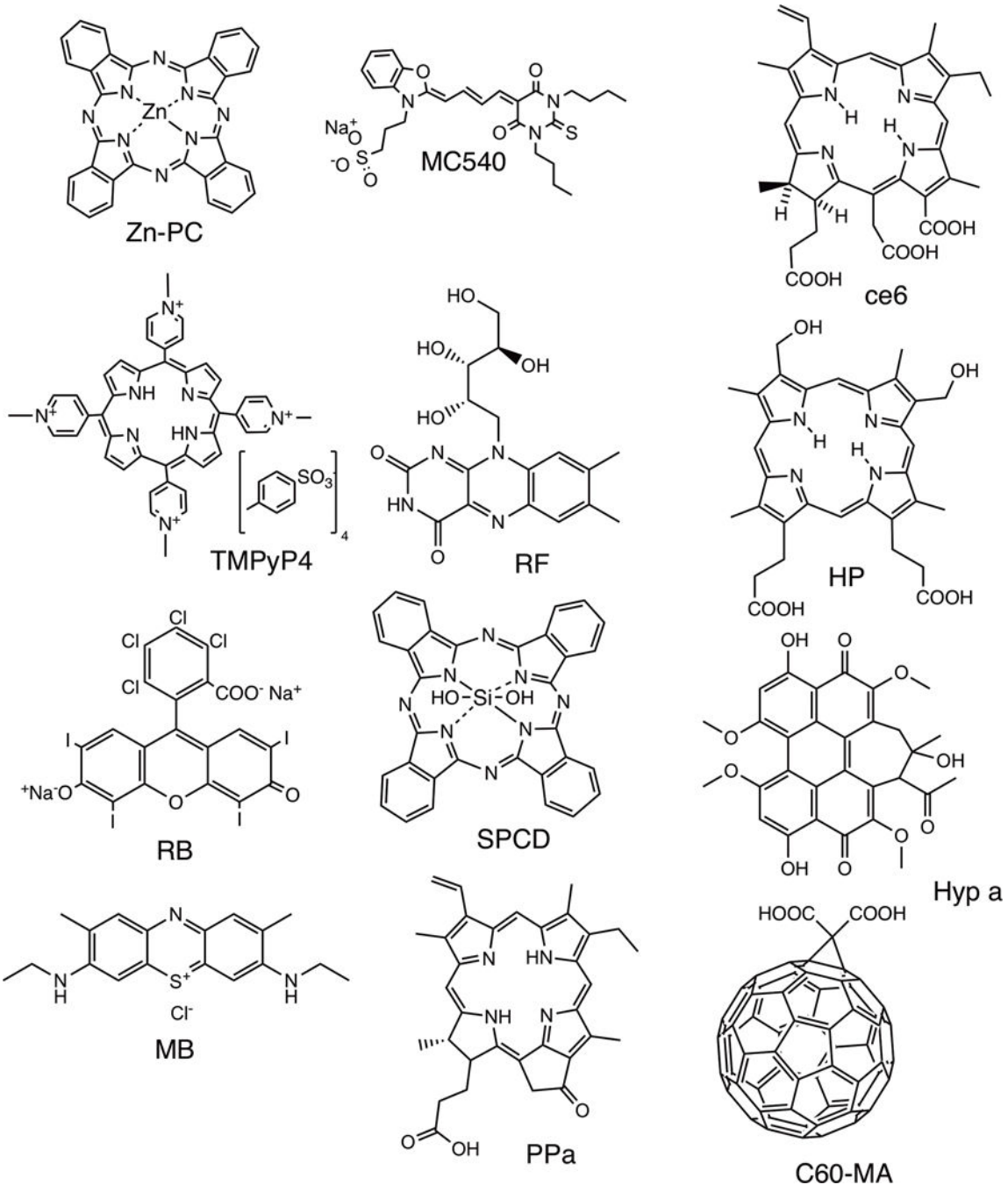

Figure 5. Chemical structures of some PS that have been employed in UCNPs

Zn-PC, zinc phthalocyanine[89]; MC540, merocyanine 540[90]; ce6, chlorin(e6)[53]; TMPyP4, tetra-(N-methyl-4-pyridyl)porphyrin tetratosylate[91]; RF, riboflavin[92]; HP, hematoporphyrin[79]; RB, Rose Bengal[94]; SPCD, silicon phthalocyanine dihydroxide[73]; Hyp a, hypocrellin a[95]; MB, methylene blue[75]; PPA, pyropheophorbide a[71]; C60-MA, C60 fullerene monomalonic acid[34].

Table 1

Reports of PDT mediated by UCNPs

UCNP (size, structure and modifications)	PS and attachment mode	Model (in vitro or in vivo)	Light (excitation and emission λ)	Authors (year)	Reference
50 nm NPs - $NaYF_4$ $MesoSiO_2$ (non-doped)	Zn-PC Non-covalent	Murine bladder cancer cells MB49	Ex 980 nm Em 541, 409, 656 nm	Guo et al (2010)	89
75 nm NPs - $MesoSiO_2$/$NaYF_4$:Yb,Er	Zn-PC plus merocyanine MC540 (single and dual loaded)	Murine melanoma cells B16-F0 in vitro, in vivo B16-F0 tumors in C57BL/6 mice	Ex 980 Em 540, 660 nm	Idris et al (2012)	90
30 nm NPs – PEG/$NaYF_4$:Yb^{3+}:Er^{3+}	Chlorin(e6), ce6 Non-covalent	HeLa human cervical and 4T1 murine breast cancer cells in vitro; in vivo 4T1 tumors in BALB/c mice	Ex 980 nm Em 550, 660 nm	Wang et al (2011)	53
15 nm NPs – PEI-$NaLuF_4$:12%Gd,50%Yb,2%Er targeted with G-quadruplex-aptamer against protein tyrosine kinase 7	Cationic porphyrin TMPyP4 (non-covalent)	CEM human T-cell acute lymphoblastic leukemia cells	Ex 980 nm Em 420, 550, 660 nm	Yuan et al (2013)	91
75 nm – core-shell $mesoSiO_2$ $NaYF_4$:Yb/Er/ Tm@$NaGdF_4$	Hematoporphyrin and docetaxel, non-covalent	4T1 cells in vitro and tumors in vivo, 980 nm combined with X-rays	Ex 980 nm Em 360, 480, 520, 550, 660 nm	Fan et al (2014)	79
26 nm meso-$NaYF_4$:Yb/Er, conjugated to folic acid and complexed with Au nanorods	Methylene blue, non-covalent	OECM-1 human oral cancer cells and tumors in nude mice	EX 980 nm Em 408, 520, 540, and 654 nm	Chen et al (2016)	75
75 nm NPs – TMAH-$NaYF_4$:Yb^{3+},Tm^{3+} (core)/ $NaYF_4$ (shell)	Riboflavin, non-covalent	SKBR3 human breast cancer cells in vitro, in vivo xenograft tumors in nude mice	Ex 975 nm Em 340, 360, 445, 475 nm	Khaydukov et al (2016)	92
50 nm NPs – core shell SiO_2-$NaYF_4$:Yb,Tm coated with TiO_2 then maleimide-PEG	Titanium dioxide, non-covalent	Human OSCC cells; imaging and PDT in tumors in nude mice	Ex 980 nm Em 350, 450 nm	Lucky et al (2015)	43
35 nm NPs-$NaGdF_4$:Yb/Nd@$NaGdF_4$:Yb/Er@$NaGdF_4$ PEG-hexaminediamine coated	Rose Bengal and - [$Pt(NH_3)2Cl_2$-($OCOCH_2CH_2NH_2)_2$] covalently conjugated	Combination chemotherapy and PDT; cisplatin sensitive/ resistant ovarian cancer cells A2780	Ex 808 nm Em 380, 410, 525, 555, 665 nm	Ai et al (2016)	72
65 nm NPs –double Meso-SiO_2 shell-$NaYF_4$:Yb/Er/Gd	Silicon phthalocyanine dihydroxide, SPCD and bioreductive drug tirapazamine. TPZ) Non-covalent	HeLa cells and xenograft tumors PDT and CT/PET imaging	Ex 980 nm Em 550, 660 nm	Liu et al (2015)	73
30 nm NPs - cationic N-octyl chitosan/$NaYF_4$:23%Yb, 2%Er@$NaYF_4$	Zn-PC Non-covalent	MRSA and *E. coli* bacteria in vitro, subcutaneous MRSA infection in CD1 mice	Ex 980 Em 660 nm	Li et al (2017)	93
53 nm NPs – PEI-$NaYF_4$:Yb/Er coated with O-carboxymethyl chitosan and targeted with RGD cyclic peptide	Pyropheophorbide a covalently conjugated	Human U87-MG glioblastoma and MCF-7 breast cancer cells	Ex 980 Em 525, 545, 665 nm	Zhou et al (2012)	71

UCNP (size, structure and modifications)	PS and attachment mode	Model (in vitro or in vivo)	Light (excitation and emission λ)	Authors (year)	Reference
20–30 nm NPs - βNaYF$_4$:Yb/Ho(8/1%)@NaYF$_4$:Nd(20%)@NaYF$_4$ core-shell-shell targeted with folate	RB covalently conjugated	HeLa cells	Ex 808 nm Em 545, 650 nm	Wang et al (2015)	94
77 nm or 112 nm NPs - PEG - NaYF$_4$:Yb,Er coated with graphene oxide quantum dots	Hypocrellin a Non-covalent	HeLa cells	Ex 980 nm Em 550, 660 nm	Choi et al (2017)	95
70 nm NPs - PEG-NaYF$_4$:Yb^{3+},Er^{3+}/NaYF$_4$:Yb^{3+},Tm^{3+} targeted with folate	monomalonic fullerene (C60MA) covalently conjugated	HeLa cells	Ex 980 Em 450, 475, 540, 650, 808 nm	Liu et al (2013)	34
25 nm NPs - PLL-NaYF$_4$:Yb/Tm	graphitic carbon nitride quantum dots (g-C3N4), non-covalent	oral epidermoid carcinoma cells (OEC-M1)	Ex 980 nm Em 345, 365, 450, 475 nm	Chan et al (2016)	52
50 nm NPs - PAA-NaGdF4:Yb,Er@Yb@Nd@Yb targeted with RGD peptide	PEG-black phosphorus nanoheets, covalently conjugated	HeLa cells, hemolysis, U14 tumors in BALB/c mice	Ex 808 nm Em 543, 654 nm	Lv et al	49
24 nmn NPs - core-shell PAA-NaYF4:Yb,Er@NaYF4	Killer red protein, covalently conjugated	MDA-MB-231 human breast cancer cells	Ex 978 nm Em 540, 660 nm	Liang et al (2017)	48